Anal Bioanal Chem (2011) 401:2103–2111
DOI 10.1007/s00216-011-5284-9

ORIGINAL PAPER

Blood cell capture in a sawtooth dielectrophoretic microchannel

Paul V. Jones · Sarah J. R. Staton · Mark A. Hayes

Received: 19 April 2011 / Revised: 18 July 2011 / Accepted: 25 July 2011 / Published online: 4 August 2011

Abstract Biological fluids can be considered to contain information-rich mixtures of biochemicals and particles that enable clinicians to accurately diagnose a wide range of pathologies. Rapid and inexpensive analysis of blood and other bodily fluids is a topic gaining substantial attention in both science and medicine. One line of development involves microfluidic approaches that provide unique advantages over entrenched technologies, including rapid analysis times, microliter sample and reagent volumes, potentially low cost, and practical portability. The present study focuses on the isolation and concentration of human blood cells from small-volume samples of diluted whole blood. Separation of cells from the matrix of whole blood was accomplished using constant potential insulator-based gradient dielectrophoresis in a converging, sawtooth-patterned microchannel. The channel design enabled the isolation and concentration of specific cell types by exploiting variations in their characteristic physical properties. The technique can operate with isotonic buffers, allowing capture of whole cells, and reproducible capture occurred at specific locales within the channel over a global applied voltage range of 200–700 V.

Keywords Dielectrophoresis · Erythrocytes · Bioparticle trapping · Separation · Blood

Abbreviations

DC	Direct current
DC-iGDEP	Direct current insulator-based gradient dielectrophoresis
DEP	Dielectrophoresis
EP	Electrophoresis
EOF	Electroosmotic flow
iDEP	Insulator dielectrophoresis

P. V. Jones · S. J. R. Staton · M. A. Hayes (✉)
Department of Chemistry and Biochemistry and Center for Solid State Electronics Research, Arizona State University,
PO Box 871604, Tempe 85287, AZ, USA
e-mail: mhayes@asu.edu

Introduction

Along with all vertebrates and many invertebrates, humans rely on blood for life. Blood is a rich, heterogeneous complex fluid that fulfills many indispensable physiological roles far beyond the realm of simple oxygen delivery. The circulatory system continuously delivers key nutrients to distant tissues of the body while simultaneously removing metabolic by-products to prevent toxic buildup. In addition, it acts as a rapid transit system for a variety of cells and chemical messengers.

Human blood is composed of two primary constituents: plasma and cells. Both of these contain diverse subgroupings of materials. The plasma is an aqueous medium composed of 90% water. Proteins contribute another 6–8% of the total, the most abundant being albumins, globulins, and fibrinogen [1]. Other solutes include a variety of ions and small molecules, such as cofactors, hormones, lipids, carbohydrates, and amino acids. Blood cells are typically classified as erythrocytes, leukocytes, or thrombocytes. Erythrocytes, or red blood cells (RBCs), constitute the vast bulk of total cell volume within the blood, making up roughly 45% of the total blood volume and accounting for more than 99% of all blood cells. RBC populations are relatively homogeneous within a single individual, but their physical characteristics can vary with blood type, cell age, and disease state [2]. Pathologies that affect red blood cells include genetic

disorders such as anemia and spherocytosis, as well as parasitic infections such as malaria [3].

The complex heterogeneity of blood and its compositional variation in response to the physiologic state of the organism make it a rich source of information. Clinicians rely on blood tests for accurate diagnosis of a wide array of diseases. Interestingly, some analytical procedures, such as the peripheral blood smear, have persisted unchanged for decades. These methods, while technologically archaic, can still yield valuable and accurate results. Their chief limitations arise from the need for experienced technologists or hematologists and the difficulty of evaluating a large number of samples from multiple individuals. Culturing or assays are often used to detect pathogens, but such approaches are time-consuming and expensive. State-of-the-art diagnostic solutions usually involve flow cytometry, which improves the accuracy and throughput of hematologic tests, but requires sophisticated laboratory facilities, expensive equipment, and trained specialists [4].

Emergent bioanalytical technologies are designed to improve upon existing methods by decreasing the time from sample collection to analysis, integrating multiple diagnostic vectors, and producing new statistically significant clinical findings while reducing costs and processing times and increasing portability. So-called lab-on-a-chip devices offer the possibility of comprehensive analysis performed at the patient's bedside—a prospect that would likely have a profound impact on the practice of medicine, especially in low-resource settings.

Electrokinetic approaches have proven extremely versatile in microfluidic applications, including separations [5]. Dielectrophoresis (DEP), in particular, provides several key benefits over other traditional separation schemes. Centrifugation, for example, can separate bioparticles based on their size and mass, but separation of particles with relatively small size differences may require high speeds and long run times [6]. Beyond the separation capabilities of centrifugation, similarly sized bioparticles often differ radically in their structure, deformability, and polarizability. Dielectrophoretic forces can uniquely couple with these physical traits, allowing sorting and capture based on far more than size or density alone [7].

Dielectrophoretic force arises when spatially varying electric fields act upon permanent or field-induced dipoles [8]. DEP is classically defined as the movement of neutral particles in a non-uniform electric field. However, DEP can also act on charged species, in combination with other electrokinetic forces such as electrophoresis (EP) and electroosmotic flow (EOF). DEP occurs in both alternating current (AC) and direct current (DC) fields. The dielectrophoretic force experienced by a particle depends on complex variables, including the particle's size, its structural and dielectric properties, and the dielectric properties of its surrounding medium. These characteristics can vary significantly between biological targets based on slight differences in their physicochemical makeup. Using DEP, seemingly similar cells can be differentiated based on subtle distinctions such as antigen type on erythrocytes or living versus dead bacteria [9, 10].

Much of the recent focus on dielectrophoretic bioseparations has emphasized the use of AC fields, attributable to known advantages such as frequency-dependent electrokinetics. Innovative researchers have studied a variety of phenomena at micro- or nanoscopic dimensions, including DEP, electrorotation, and dielectric levitation [11–13]. Both novel and informative, many of these techniques enable the analysis of small, even single-cell samples [14]. However, these devices often leave unsolved the problems of sample dilution, continuous high-throughput testing, or truly diverse and complex biological samples.

In 2003, Cummings [15] described the use of insulating features in a microchannel to shape DC electric fields and generate DEP forces. This work complemented analogous innovations using insulators and AC electric fields [16]. While the more traditional electrode-based DEP allowed large electrical gradients to form with lower voltages, insulator-based dielectrophoresis (iDEP) allowed placement of the electrodes in remote reservoirs, eliminating problems created by electrochemical reactions in the gradient zone. Various implementations of iDEP have been demonstrated over the past few years using features such as glass beads, nanopipettes, insulating hurdles, and serpentine channels [17–20]. Another commonly recurring design features a series of uniformly sized insulating posts along the length of a channel [21–23]. In this case, the posts shape non-uniformities in the electric field and create DEP traps.

The research presented here utilized insulating sawtooth shapes along the edge of a microchannel to create electric field variations. DC fields were used to drive bulk motion of the sample as well as create dielectrophoresis-inducing field non-uniformities. Rather than being driven hydrodynamically, particles were thus propelled down-channel through a combination of EP and EOF. The superposition of these electrokinetic forces allows differentiation and, therefore, analysis of a wider variety of particles than EP or DEP alone. The sawtooth pattern facilitates the formation of differing and distinct local gradients, or DEP traps, along the overall channel length. This induces particles to stop at unique points along the device based on their characteristic electrophoretic and dielectrophoretic properties. To investigate the application of a potentially inexpensive and portable DC insulator gradient DEP platform for blood-based diagnostics, whole blood samples were tested within such a device. Red blood cells were successfully and reproducibly captured within a spatially confined section of the sawtooth microchannel. Some cells were observed to

pass through these sections, supporting the existence of subpopulations with lower ratio of dielectrophoretic mobility (μ_{DEP}) to electrophoretic mobility (μ_{EP}) than captured cells. Future modifications to insulator geometry may enable differentiated isolation of such subpopulations. Although this possibility is underscored by recent papers which describe dielectrophoretic characterization of RBCs based on cell age [24] and ABO antigen type [9], such efforts have all revolved around the use of electrode-based DEP. This work marks the first attempt to capture and isolate RBCs using DC-iDEP.

Materials and methods

As a brief overview, experiments were conducted in microfluidic devices constructed from glass and polydimethylsiloxane (PDMS). Blood cells suspended in isotonic phosphate buffer were introduced into the channel from one end. External platinum electrodes connected to a high-voltage power supply were inserted into access reservoirs at each end of the microchannel and used to apply a DC potential (ΔV_{global}) across the entire device (Fig. 1). RBCs and other materials were transported and captured within the channel.

Microdevice fabrication

Microfluidic devices were fabricated using adaptations of standard soft lithographic techniques [25]. Microchannel templates were created on Si wafers with AZ P4620 positive photoresist (AZ Electronic Materials, Branchburg, NJ) and contrast enhancement material CEM388SS (Shin-Etsu MicroSi, Inc., Phoenix, AZ) [7, 21]. The resist was exposed via contact photolithography with a photomask designed and created using AutoCAD (Autodesk, Inc., San Rafael, CA). PDMS (Sylgard 184, Dow/Corning, Midland, MI) was poured over the template and allowed to cure for 1 h at 70 °C. Afterwards, 2-mm diameter access holes were punched through the PDMS to access reservoirs at each end of the microchannel. The imprinted PDMS surface was oxidized using a handheld corona discharge emitter (Electro-Technic Products, Inc., Chicago, IL) set to 50 kV. The PDMS slab was then contact-sealed to a glass coverplate, which had previously been triple-washed with an Alconox solution, rinsed with 18 MΩ water and 100% isopropyl alcohol, then dried for 6 h at 450 °C.

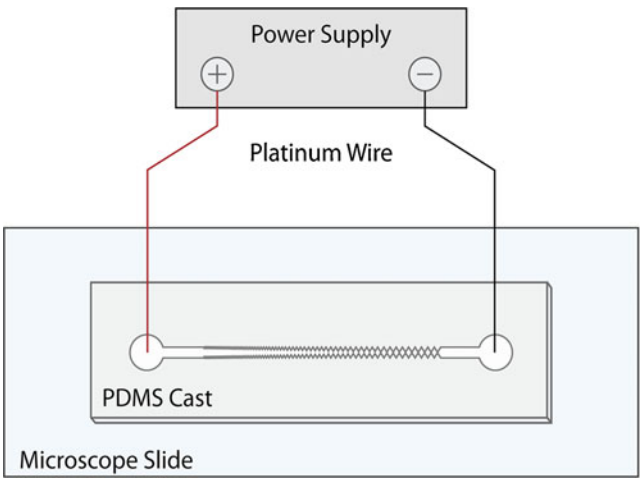

Fig. 1 Schematic of the apparatus used in these experiments. A high-voltage DC power supply was used to generate field potentials within the microchannel. Platinum wires were inserted into access reservoirs punched through the PDMS cast. A microscope slide or a glass plate was used to seal the channel following oxygen plasma treatment of the PDMS surface

The microchannel geometry was composed of successively larger, equilateral triangular units lining each side of the channel [26]. The apex of each triangle coincided with another on the opposite side, forming sequentially narrower gaps, or gates, along a gradually converging sawtooth pattern. The smallest triangles consisted of 6-μm sides and a 5.2-μm height. The side length of the triangles increased by 40 μm after every sixth repeat. This yielded an overall design with an initial gate width of 945 μm and a final gate width of 27 μm. The whole channel length was 4.1 cm with an average depth of 14±1 μm.

Sample preparation

Fresh whole blood was obtained from a human donor by venipuncture or capillary blood draw. Samples obtained via venipuncture were collected in vacutainers containing 1.8 mg/mL K_2EDTA and stored in a refrigerator at 4 °C for up to 4 days. Samples obtained via fingerstick were collected in a microcentrifuge tube containing 1 mL isotonic sodium phosphate buffer with EDTA. Samples obtained in this manner were used within a few hours of collection. In certain experiments, diluted whole blood was used for analysis. In others, the sample was centrifuged and cells were washed with additional phosphate buffer to remove plasma and serum proteins.

For staining, blood cells were suspended in buffer containing 5 μM Vybrant DiO dye (Invitrogen, Inc., Carlsbad, CA) at 0.5% hematocrit. Excitation and emission wavelengths for this dye are 484 and 501 nm, respectively. The sample was incubated for 15 min at 37 °C, then centrifuged, and washed three times in order to remove free dye molecules. The final cell pellet was resuspended in sodium phosphate buffer, pH 7.4, with concentrations typically between 100 and 130 mM. Conductivities for these buffers were 12.5 and 15.5 mS/cm, respectively. Sufficient buffer was added to yield an absolute cell count of 22–56 cells/nL based on a presumed mean corpuscular volume (MCV) of 90 fL [27]. This MCV

corresponds with the typical RBC disk diameter of 6–8 μm and thickness of 2 μm.

Experimental procedure

A small amount of buffer was pipetted into the sample port on the wide-gated end of the channel, hereafter referred to as the inlet reservoir, allowing the channel to fill passively via capillarity. The device was inspected under optical magnification for uniform fluid distribution, absence of debris, and well-formed microstructures. A blood sample was then pipetted into the inlet reservoir. Once cells had entered the device hydrodynamically, achieving uniform distribution within the channel, buffer was added to the opposite access port to balance the hydrodynamic pressure. The loaded device was then situated on top of a microscope stage. Platinum electrodes (0.404-mm external diameter, 99.9% purity, Alfa Aesar, Ward Hill, MA) were inserted through the access ports into the terminal reservoirs and connected via alligator clips to a Series 225 DC power supply (Bertan High Voltage Corp., Hicksville, NY).

Data collection and mathematical modeling

Experiments were observed on an Olympus IX70 inverted microscope with a ×4 or ×10 objective. Samples were illuminated with a mercury short arc lamp (H30 102 w/2, OSRAM) and an Olympus DAPI, FITC, Texas Red triple band-pass cube (Olympus, Center Valley, PA). Videos and still images were collected with a monochrome QICAM cooled CCD camera (QImaging, Inc., Surrey, BC) and Streampix III image capture software (Norpix, Inc., Montreal, QC).

The electric field within the microdevice was numerically modeled with COMSOL Multiphysics software (COMSOL, Inc., Burlington, MA). The model utilized properly scaled geometry of the main channel. A simplified 2D approximation was used since the electrical potential is presumed invariant across the depth of the microchannel. The conductivity and relative permittivity of the medium were set to 1.2 S/m and 78, respectively. Electric field properties were evaluated for a ΔV_{global} of 550 V.

Safety considerations

All experiments were carried out in a Biosafety Level II laboratory, with approval from the Institutional Review Board for human subjects.

Results

The behaviors of several different complex biological samples associated with blood were examined on the DC insulator gradient dielectrophoretic (DC-iGDEP) device, including diluted whole blood, washed cells, isolated RBCs, and diluted blood plasma. Capture of RBCs and other particles was investigated while varying the buffer and globally applied potential. During the course of the experiments, buffers were varied between 100 and 130 mM sodium phosphate maintained near a physiological pH of 7.4, and ΔV_{global} was varied from 200 to 700 V (49–171 V/cm). These buffer concentrations correspond roughly to osmolarities of 225–325 mOsM, thus bracketing the mean physiological value of 289 mOsM for human serum [28]. The ionic strength of the suspension buffer was varied to some extent, but significant departures from isotonicity resulted in hemolysis. Suspension in near-isotonic buffers reduces the osmotic pressure, minimizing stress and deformation of erythrocytes. A limited number of experiments were performed using buffer concentrations as low as 20 mM (σ=0.38 mS/cm), but rapid lysing during sample preparation and experimentation restricted the range of observations.

Certain characteristic behaviors were observed in nearly all experiments (Fig. 2). Immediately after a DC potential was applied to the channel, particles moved toward the outlet reservoir, where the negative electrode was located. Removal of the potential caused all observable motion to cease immediately. Little or no particle capture was detected in the wider segments of the channel. Instead, cells and debris in these regions followed continuous paths toward the outlet. The path lines traced by these particles exhibited a marked similitude to the electric field lines modeled from the channel geometry. At narrow gates, cells and other particles appeared to divert from field path lines and become trapped (note that Fig. 3 presents field contours, not field lines—lines are perpendicular to contours). In these cases, particles were seen to stop both centrally, within the suspending medium, and peripherally, at or near the channel walls.

Two general types of capture were observed within the sawtooth channel (Fig. 4), and they are defined here for clarity of the narrative rather than any distinct physical feature or process. Type 1 capture was observed first. In this scenario, RBCs began to collect near the channel centerline. These RBCs appeared to be whole and unfragmented, resisted bulk fluid motion, appeared to float freely in solution, and aggregation between particles was minimal. In some cases, the captured RBCs formed short pearl chains of three to six cells axially oriented along field lines. Type 1 capture commenced immediately after the application of a sufficient global potential. Collection occurred immediately upstream of the 27-μm gates, which are located nearest to the channel outlet. Type 2 capture involved smaller particles (including fragmented RBCs) which exhibited different electrokinetic behavior by collecting primarily at the apices

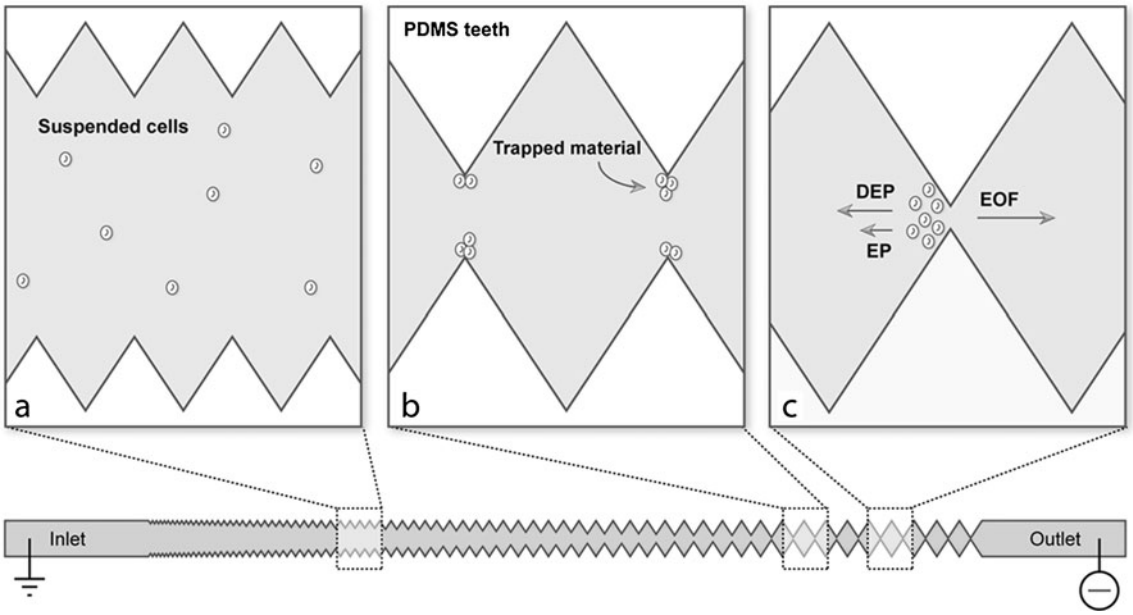

Fig. 2 Schematic representation of the patterned microchannel showing unhindered passage (**a**), type 2 capture (**b**), and type 1 capture (**c**) of RBCs

of PDMS teeth. Particles captured in this manner exhibited a high degree of aggregation. Type 2 capture was observed only after 3–5 min of applied voltage. Under typical experimental conditions, this behavior was observed primarily at 97-μm gates, located upstream from the primary site of type 1 capture.

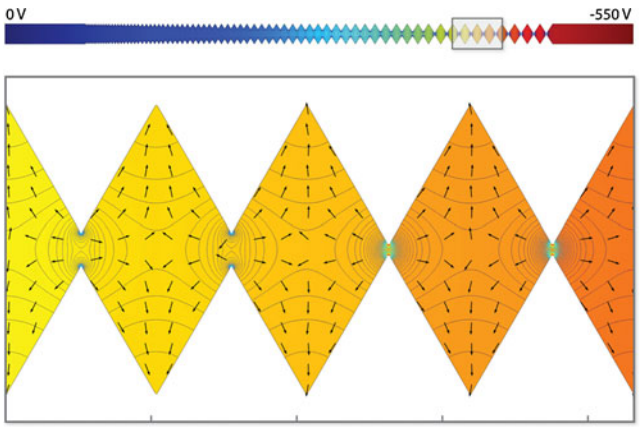

Fig. 3 Model showing electrical field properties within the channel computed using COMSOL Multiphysics. In this representation, the *solid colored surface* represents the local potential, *contour lines* correspond to the magnitude of the electric field (E), and *arrows* (normalized) indicate the direction of dielectrophoretic force (proportional to $\nabla|\mathbf{E}|^2$) for negative DEP. Under the conditions used in these experiments, EOF was the primary driving force, causing RBCs to move from the inlet to the outlet reservoir. As particles travel through successively narrower gates, they encounter increasing DEP forces. When a particle reaches a gap with a sufficiently large gradient, the DEP overcomes the other electrokinetic forces, effectively trapping the particle at that site

Unstained blood samples were used to determine the effect of carbocyanine dye (Vybrant DiO) on DEP capture in these samples. Brightfield microscopy was used to verify that both type 1 and type 2 capture occurred with unstained samples when all other factors were held constant (Fig. 5).

The voltage dependence of capture was investigated by varying ΔV_{global} in multiple trials (Fig. 6). Electrokinetic capture was most evident and reproducible when ΔV_{global} ranged between 500 and 600 V. At lower potentials, capture zones appeared to destabilize or shift downstream (toward the outlet). Type 1 capture of whole cells was only observed when ΔV_{global} exceeded 200 V. Below this value, no type 1 capture was observed, and type 2 capture shifted down-channel from the 97-μm gates to the 27-μm gates. At higher potentials, RBCs were more prone to rupture and fragment.

In many experiments, the abundance of small particles moving down-channel from the inlet reservoir increased with time. After 10 to 15 min at high ΔV_{global}, the aggregates grew large enough to plug the first 27-μm gate. Saturation, or complete blockage in this manner, led to the rapid, nonspecific accumulation of solid material at that gate. This effect was investigated further by lysing RBC samples in a hypotonic buffer solution prior to microfluidic analysis. Dynamic light scattering revealed that the mean fragment size after buffer-induced hemolysis was approximately 2.5 μm, compared to a mean diameter of 6–8 μm for whole RBCs. Experimental surveillance of these samples at field potentials of 500–600 V yielded results consistent with type 2 capture. No type 1 capture was observed (Fig. 7).

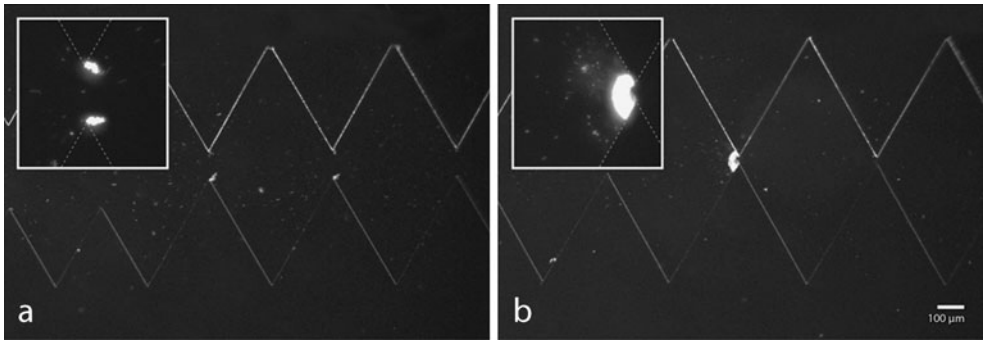

Fig. 4 Cell capture in a narrow channel segment. **a** In type 2 capture, material collects near the apices of the PDMS teeth while other cells and particles continue to flow unhindered from left to right. The gate width shown here is 97 µm. *Inset* shows a magnified view. **b** In type 1 capture, cells are captured upstream of the gate. After several minutes of collection, a plug forms and saturates the gate. Farther upstream, cells continue to flow toward the outlet until they reach the saturation site. The gate width shown here is 27 µm. *Inset* shows a magnified view

Discussion

The use of DC fields to drive particle motion within a shaped insulating (glass or PDMS) microstructure gives rise to complex phenomena. According to basic DEP theory, three primary variables are relevant for simple spheres in a DC field: the gradient of the square of the electric field ($\nabla|\mathbf{E}|^2$), the particle radius, and the conductivities of the particle (σ_p) and medium (σ_m) [29]. DEP force is proportional to the former two variables, while the sign of the resulting vector force is described by the Clausius–Mossotti relation, a mathematical term describing the relative conductivities of the particle and the medium. Depending on the conductivity of the particle and its surrounding medium, the DEP force will either be oriented in the direction of increasing or decreasing field strength. This describes positive dielectrophoresis (pDEP) and negative dielectrophoresis (nDEP), respectively. For small particles, EP force is proportional to a particle's net surface charge and the electric field strength. At physiological pH, RBCs have a net negative charge, so the EP force will be directed along field lines toward the positive electrode [30]. The negatively charged surfaces of glass and oxidized PDMS will cause EOF directed toward the negative electrode. In channel configurations with low Reynolds number, EOF also follows electric field lines [31]. Under these experimental conditions, EOF contributes more significantly to translational forces than EP. This is consistent with the observed motion of particles toward the outlet reservoir, which houses the negative electrode. Furthermore, particles distant from the capture zones followed scalloped path lines similar to model electric field lines and contours (Fig. 3). Despite dominant EOF, the electrophoretic mobility (μ_{EP}) of a given particle will still influence its behavior within the channel. Explicitly, particle capture zones depend on the ratio $\mu_{DEP}/(\mu_{EO}+\mu_{EP})$ [32].

Capture of RBCs and other material correlates well with existing models [32] and basic theories of DEP. The PDMS teeth within the channel impinge locally upon the passage of current induced by the globally applied electric potential. This creates intense, local field gradients with the greatest magnitude near the vertices (Fig. 3). An approaching particle with negative μ_{DEP} will experience a repulsive DEP force, directed away from the vertices and the transverse midline of the gate, while a particle with positive μ_{DEP} will experience an oppositely directed attractive force. As a particle travels down-channel, it moves into and out of sequentially increasing local gradients. If a particle's μ_{DEP} is small or the gates are wide, the combined force of EP and EOF will exceed that of DEP. Under these conditions, the

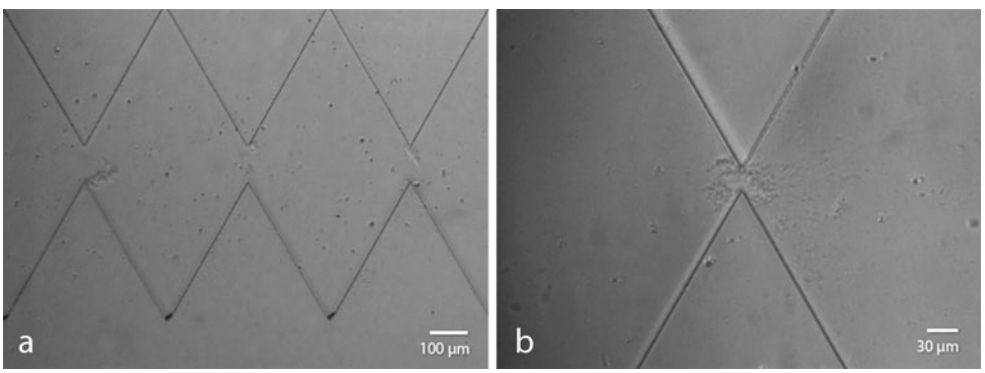

Fig. 5 Capture of unlabeled (dye-free) cells. **a** Type 2 capture is observed with an unstained blood sample at 97-µm gates. The refractive index of cells and biomaterials differs from that of the surrounding medium, allowing visualization with simple bright field microscopy. **b** Saturation of a 27-µm gate is shown under similar conditions

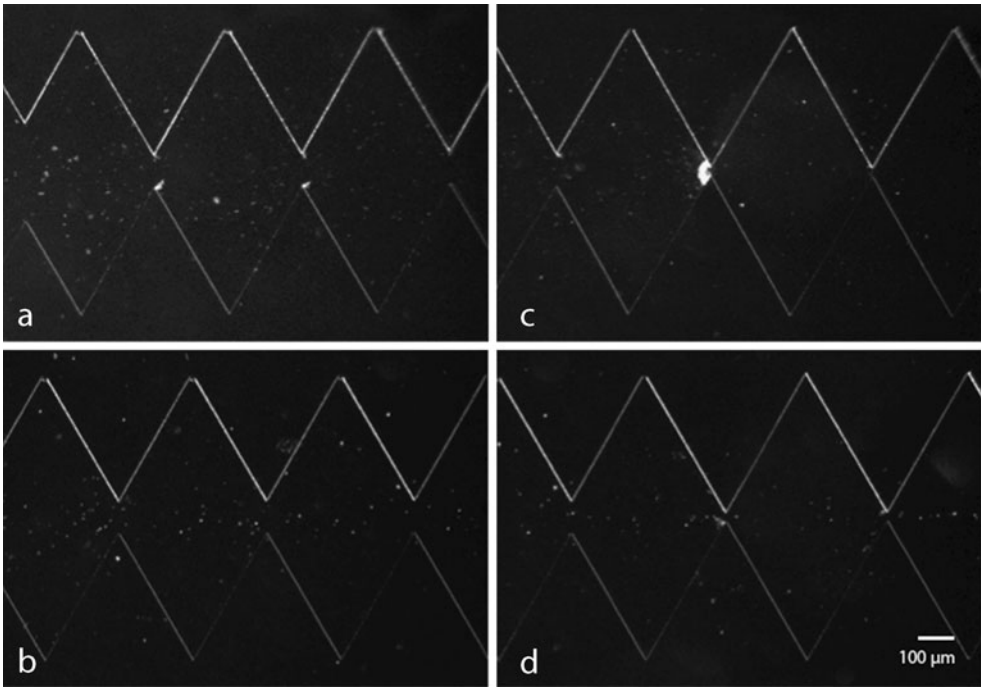

Fig. 6 Differences in cell capture based on global potential and gate width. **a** 550 V. Type 2 capture is observed at 97-µm gates. **b** 200 V. At lower potentials, no capture is observed at 97-µm gates. **c** 550 V. Type 1 capture has caused cells to accumulate at a 27-µm gate, contributing to near-saturation of that gate. **d** 200 V. At lower potentials, no type 1 capture was observed. Type 2 capture, however, now occurs at the 27-µm gates. t=15 min for all images

particle will pass the gate and travel continuously toward the device outlet. If, however, μ_{DEP} is large or the gate is sufficiently narrow, DEP can overcome the other forces, resulting in particle capture. Type 1 capture consisted of RBC trapping upstream of a given gate, indicating gradient-induced repulsion resulting from nDEP. Type 2 capture occurred at the tips of PDMS teeth, consistent with pDEP. Other researchers have demonstrated nDEP with erythrocytes in low-frequency AC fields and determined that this effect is expected when erythrocyte electrical conductivities are modeled as a single-shell oblate sphere [33]. This behavior is likely governed by the low conductivity of the RBC membrane relative to the cytosol and surrounding medium. Also observed in association with nDEP capture was the alignment of cells into short pearl chains. Pearl chain formation with RBCs has been observed in both AC and DC applications of DEP [34]; it is attributed to the induced polarization of cells and subsequent dipole–dipole interactions, along with micro-heterogeneities in the electric field created by the cells [35]. At the voltages used in these experiments, a small number of cells (typically <10%) passed uncaptured through the final sets of 27-µm teeth. Since these teeth create the strongest DEP traps within the device, the uncaptured cells represent a subset of the population with either lower μ_{DEP} or higher μ_{EP} than the others. Such electrokinetic variability can be attributed to slight differences in the physical properties of RBCs such as size, rigidity, or the expression of surface proteins.

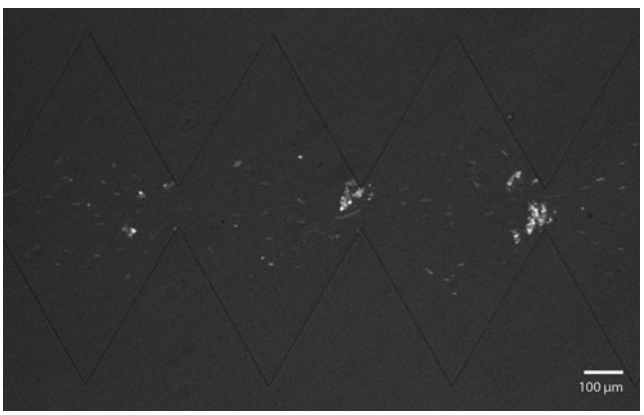

Fig. 7 Capture of pre-lysed RBCs. Fluorescence microscopy of RBC fragments in the microchannel revealed trapping and aggregation of particles consistent with type 2 capture. Dynamic light scattering established a mean initial particle diameter of 2.5 µm

Repeated trials with varied electric field strength demonstrated that appreciable capture only occurs above a certain threshold voltage. The magnitude of local electric field strength is proportional to the globally applied potential and inversely proportional to the cross-sectional area of the channel. Altering ΔV_{global} will change local magnitudes of $\nabla|\mathbf{E}|^2$ and the resulting DEP force. When ΔV_{global} was <200 V, the dielectrophoretic force was insufficient to effectively capture cells and cell fragments. Perhaps more interesting was an apparent shift of capture up- or down-channel with a respective increase or decrease in ΔV_{global}. pDEP capture, for example, was observed at 97-µm gates when ΔV_{global} exceeded 500 V, but occurred exclusively at 27-µm gates as ΔV_{global} approached 200 V.

Most experiments were visualized via fluorescence microscopy. Labeling the membranes of RBCs and other

cells with a lipophilic carbocyanine dye (Vybrant DiO) facilitated convenient detection and monitoring. While the dye molecules are positively charged, control experiments with unlabeled blood and RBC samples established that capture was not dependent on the inclusion of intercalated dye molecules within whole or fragmented cell membranes.

Localized accumulation of bioanalyte was typically evident within 1 min of ΔV_{global} application. Selective accretion usually continued for 10–15 min, until enough material had collected to span the width of the channel. Continued buildup at such saturation points was presumed to be nonspecific and indicated that the blockage site was still permeable to aqueous buffer since upstream particle motion was still consistent with EOF-driven bulk flow. These results are promising since selective and localized capture occurred within a short timescale. At the voltages used in these experiments, RBCs began to lyse after 5–10 min of continuously applied potential. Observed via fluorescence, lysis was noted by observing a marked decrease in fluorescence intensity of the particulates associated with erythrocyte morphology, accompanied by the appearance of increasingly abundant debris and small fragments. Lysis always began at the narrow end of the channel taper then gradually progressed upstream. Under certain conditions, an erythrocyte's membrane may be perforated or torn while retaining some of its overall physical structure. Once the bilayer integrity has been compromised and the cytoplasm is lost, the remaining shell is referred to as a ghost [36]. RBC ghosts and other cell fragments exhibited different electrokinetic behavior than intact RBCs—they were both more likely to participate in pDEP capture. Another distinction was the greater degree of particle aggregation observed in this scenario. Whole cells appeared to engage primarily in nDEP capture. Very little particle aggregation occurred apart from pearl chain formation. Cells captured in this manner had not simply adhered to the glass or PDMS surfaces, which was confirmed by observing their release from capture zones upon removal of the applied electric field.

Cell lysis may have resulted from Joule heating resulting from the use of relatively high-conductivity buffers and a low heat transfer configuration compared to other electrophoretic techniques [37, 38]. Greater electrical resistance across the narrowest gates induces concentrated power dissipation, resulting in local heating in this section of the channel and forming a longitudinal temperature gradient, somewhat offset by the high surface area-to-volume ratio of these sections. This local heating provides one possible explanation for the progressive lysis of RBCs as they move down-channel. If Joule heating does indeed cause or contribute to the destruction of cells, these effects might be ameliorated by the use of low-conductivity zwitterion buffers or altered heat dissipation strategies [24]. Since EOF appeared to be a strong contributor to the overall fluid velocity within the channel, reducing the zeta potential of the channel walls will also reduce the field strength required for particle capture [39]. Dynamic surface coatings can decrease the electric field strength required for particle capture while maintaining the biocompatible nature of iDEP-based techniques [40].

Methods for isolating or selectively staining WBCs and platelets were not pursued for this study. Instead, we focused on capturing a single analyte (RBCs) from a complex biological fluid in the form of diluted whole blood. Favorable comparisons were observed between samples enriched for RBCs and samples in which no such enrichment occurred. Trials with human serum samples further established that the ability to capture RBCs was not dependent on the presence or absence of other fluid components such as serum proteins or cofactors. Spatially resolved separation of blood's distinct cellular components within a single channel may be possible with iterative modeling and design improvements. Optimization of channel geometry, surface treatments, and buffer composition all promise to augment the bioseparatory power of this technique. Promising results recently generated in this laboratory indicate this possibility, with spatially resolved separation of bacteria [7], fluorescent microspheres [26], and amyloid Aβ protein fibrils [41].

Conclusion

The strategy investigated here exploited specific insulator geometry and a DC field to facilitate capture of RBCs from samples of human blood. This work is an extension of iDEP technology pioneered within the last decade and demonstrates the first known capture of RBCs using insulators and DC fields. Electric field modeling demonstrated that capture zones coincided with areas of high DEP force. Further modeling of channel geometry and bioparticle physics will enable optimization of DC-iGDEP devices for the separation of bioanalytes from complex, naturally heterogeneous fluids. Future applications may include isolating pathogens from blood or identifying variants within a single cell type (such as RBCs).

Refinement of the physical characteristics of the device will lead to the development of clinical bioanalytical tools. The simple glass–PDMS construction used here demonstrates that favorable results can be obtained with DC fields and inexpensive, disposable materials. Treatment with surface coatings to modulate EOF (and reduce fouling) will likely improve results further. In the future, engineering of DC-based microdevices may eliminate the need for bulky power supplies and allow the construction of portable, battery-operated diagnostic tools.

References

1. Sherwood L (2010) Human physiology: from cells to systems, 7th edn. Brooks/Cole, Belmont
2. Zuckerman KS (2007) In: Goldman L, Ausiello D (eds) Cecil medicine, 23rd edn. Saunders, Philadelphia
3. Greer JP, Foerster J, Rodgers GM, Paraskevas F, Glade B, Arber DA, Means RT (eds) (2008) Wintrobe's clinical hematology, 12th edn. Lippincott Williams & Wilkins, Philadelphia
4. Toner M, Irimia D (2005) Blood-on-a-chip. Annu Rev Biomed Eng 7:77–103
5. Meighan MM, Staton SJR, Hayes MA (2009) Bioanalytical separations using electric field gradient techniques. Electrophoresis 30:852–865
6. Cabrera C, Yager P (2001) Continuous concentration of bacteria in a microfluidic flow cell using electrokinetic techniques. Electrophoresis 22(2):355–362
7. Pysher MD, Hayes MA (2007) Electrophoretic and dielectrophoretic field gradient technique for separating bioparticles. Anal Chem 79(12):4552–4557
8. Pohl HA (1951) The motion and precipitation of suspensoids in divergent electric fields. J Appl Phys 22(7):869–871
9. Srivastava SK, Daggolu PR, Burgess SC, Minerick AR (2008) Dielectrophoretic characterization of erythrocytes: positive ABO blood types. Electrophoresis 29(24):5033–5046
10. Lapizco-Encinas B, Simmons B, Cummings E, Fintschenko Y (2004) Dielectrophoretic concentration and separation of live and dead bacteria in an array of insulators. Anal Chem 76(6):1571–1579
11. Lapizco-Encinas BH, Rito-Palomares M (2007) Dielectrophoresis for the manipulation of nanobioparticles. Electrophoresis 28:4521–4538
12. West J, Becker M, Tombrink S, Manz A (2008) Micro total analysis systems: latest achievements. Anal Chem 80(12):4403–4419
13. Gascoyne P, Satayavivad J, Ruchirawat M (2004) Microfluidic approaches to malaria detection. Acta Trop 89(3):357–369
14. Thomas RS, Morgan H, Green NG (2009) Negative DEP traps for single cell immobilisation. Lab Chip 9(11):1534–1540
15. Cummings EB (2003) Streaming dielectrophoresis for continuous-flow microfluidic devices. IEEE Eng Med Biol Mag 22(6):75–84
16. Chou CF, Tegenfeldt JO, Bakajin O, Chan SS, Cox EC, Darnton N, Duke T, Austin RH (2002) Electrodeless dielectrophoresis of single- and double-stranded DNA. Biophys J 83:2170–2179
17. Suehiro J, Zhou G, Imamura M, Hara M (2003) Dielectrophoretic filter for separation and recovery of biological cells in water. IEEE Trans Ind Appl 39(4):1514–1521
18. Ying L, White SS, Bruckbauer A, Meadows L, Korchev YE, Klenerman D (2004) Frequency and voltage dependence of the dielectrophoretic trapping of short lengths of DNA and dCTP in a nanopipette. Biophys J 86:1018–1027
19. Kang Y, Li D, Kalams SA, Eid JE (2008) DC-dielectrophoretic separation of biological cells by size. Biomed Microdevices 10:243–249
20. Zhu J, Tzeng TRJ, Hu G, Xuan X (2009) DC dielectrophoretic focusing of particles in a serpentine microchannel. Microfluid Nanofluid 7:751–756
21. Cummings E, Singh A (2003) Dielectrophoresis in microchips containing arrays of insulating posts: theoretical and experimental results. Anal Chem 75(18):4724–4731
22. Lapizco-Encinas B, Davalos R, Simmons B, Cummings E, Fintschenko Y (2005) An insulator-based (electrodeless) dielectrophoretic concentrator for microbes in water. J Microbiol Methods 62(3):317–326
23. Baylon-Cardiel JL, Lapizco-Encinas BH, Reyes-Betanzo C, Chavez-Santoscoy AV, Martinez-Chapa SO (2009) Prediction of trapping zones in an insulator-based dielectrophoretic device. Lab Chip 9(20):2896–2901
24. Gagnon Z, Gordon J, Sengupta S, Chang HC (2008) Bovine red blood cell starvation age discrimination through a glutaraldehyde-amplified dielectrophoretic approach with buffer selection and membrane cross-linking. Electrophoresis 29(11):2272–2279
25. Mack C (2007) Fundamental principles of optical lithography: the science of microfabrication. Wiley, Chichester
26. Staton SJR, Chen KP, Taylor TJ, Pacheco JR, Hayes MA (2010) Characterization of particle capture in a sawtooth patterned insulating electrokinetic microfluidic device. Electrophoresis 31 (22):3634–3641
27. Turgeon ML (2004) Clinical hematology: theory and procedures, 4th edn. Lippincott Williams & Wilkins, Philadelphia
28. Hendry E (1961) Osmolarity of human serum and of chemical solutions of biologic importance. Clin Chem 7(2):156–164
29. Pohl HA (1978) Dielectrophoresis: the behavior of neutral matter in nonuniform electric fields. Cambridge University Press, Cambridge
30. Jan K, Chien S (1973) Role of surface electric charge in red blood-cell interactions. J Gen Physiol 61(5):638–654
31. Cummings EB, Griffiths SK, Nilson RH, Paul PH (2000) Conditions for similitude between the fluid velocity and electric field in electroosmotic flow. Anal Chem 72:2526–2532
32. Chen KP, Pacheco JR, Hayes MA, Staton SJR (2009) Insulator-based dielectrophoretic separation of small particles in a sawtooth channel. Electrophoresis 30(9):1441–1448
33. Pethig R (2010) Dielectrophoresis: status of the theory, technology, and applications. Biomicrofluidics 4(2):022811
34. Minerick A, Zhou R, Takhistov P, Chang H (2003) Manipulation and characterization of red blood cells with alternating current fields in microdevices. Electrophoresis 24(21):3703–3717
35. Wong P, Wang TH, Deval JH, Ho CM (2004) Electrokinetics in micro devices for biotechnology applications. IEEE/ASME Trans on Mechatronics 9(2):366–376
36. Mohandas N, Gallagher PG (2008) Red cell membrane: past, present, and future. Blood 112(10):3939–3948
37. Grushka E, McCormick RM, Kirkland JJ (1989) Effect of temperature gradients on the efficiency of capillary zone electrophoresis separations. Anal Chem 61:241–246
38. Tang GY, Yan DG, Yang C, Gong HQ, Chai CJ, Lam YC (2006) Joule heating and its effects on electroosmotic flow in microfluidic channels. J Phys Conf Ser 34:925–930
39. Martinez-Lopez JI, Moncada-Hernandez H, Baylon-Cardiel JL, Martinez-Chapa SO, Rito-Palomares M, Lapizco-Encinas BH (2009) Characterization of electrokinetic μ_{DEP} of microparticles in order to improve dielectrophoretic concentration. Anal Bioanal Chem 394(1):293–302
40. Davalos RV, McGraw GJ, Wallow TI, Morales AM, Krafcik KL, Fintschenko Y, Cummings EB, Simmons BA (2008) Performance impact of dynamic surface coatings on polymeric insulator-based dielectrophoretic particle separators. Anal Bioanal Chem 390 (3):847–855
41. Picou R, Moses JP, Wellman AD, Kheterpal I, Gilman SD (2010) Analysis of monomeric Aβ (1-40) peptide by capillary electrophoresis. Analyst 135(7):1631–1635